Thioflavin T templates Amyloid β(1-40) Conformation and Aggregation pathway

Maria Giovanna Di Carlo [a], *Velia Minicozzi* [b,*], *Vito Foderà* [c,*], *Valeria Militello* [a], *Valeria Vetri* [a,*], *Silvia Morante* [b], *and Maurizio Leone* [a]

[a] Dipartimento di Fisica e Chimica, Università degli Studi di Palermo, Via Archirafi 36, I-90123 Palermo, Italy

[b] Dipartimento di Fisica, Università degli Studi di Roma "Tor Vergata" and INFN, Via della Ricerca Scientifica 1, I-00133 Roma, Italy

[c] Section for Biologics, Department of Pharmacy, University of Copenhagen, Univeristetsparken 2, DK-2100 Copenhagen, Denmark

CORRESPONDING AUTHOR FOOTNOTE: *To whom correspondence should be addressed.

Vito Foderà
University of Copenhagen,
Univeristetsparken 2,
DK - 2100, Copenhagen, Denmark
Phone: +45 35 33 61 31
Email: vito.fodera@sund.ku.dk.

Velia Minicozzi
Università degli Studi di Roma "Tor Vergata"
Via della Ricerca Scientifica 1,
I-00133, Roma, Italy
Phone: +390672594554
Email: minicozzi@roma2.infn.it

Valeria Vetri
Università degli Studi di Palermo
Viale delle scienze Edificio 18,
I-90128, Palermo, Italy
Phone: +3909123891782
Fax: +390916234281
Email: valeria.vetri@unipa.it

Abstract

Aβ(1-40) peptide supramolecular assembly and fibril formation processes are widely recognized to have direct implications in the progression of Alzheimer's Disease. The molecular basis of this biological process is still unknown and there is a strong need of developing effective strategies to control the occurring events. To this purpose the exploitation of small molecules interacting with Aβ aggregation represents one of the possible routes. Moreover, the use specific labeling has represented so far one of the most common and effective methods to investigate such a process. This possibility in turn rests on the reliability of the probe/labels involved.

Here we present evidences of the effect of Thioflavin T (ThT), a worldwide used fluorescent dye to monitor amlyloid growth, on the Aβ(1-40) conformation, stability and aggregation. By combining experimental information and molecular dynamics simulation results, we show that the presence of ThT in solution affects peptide conformation inducing peculiar supramolecular association. In particular ThT interactions with specific Aβ(1-40) residues promotes a rigid partially-folded conformation which shifts the balance between different species in solution toward a more aggregation-prone ensemble of peptides, leading to aggregation. Our findings suggest ways for developing strategies to reverse and block aggregation or to stimulate supramolecular assembly and consequently reduce the presence of transient oligomers. This investigation underlines the need of developing label-free techniques for unbiased quantitative studies of Aβ(1-40) aggregation processes.

Keywords: Alzheimer´s disease, Thioflavin T, Aβ(1-40) Peptide, Protein Aggregation, Protein Conformation, Secondary Structure.

A significant number of high-impact human pathologies, such as Alzheimer's, Parkinson's and Huntington's diseases, are characterized by the presence either in intracellular or extracellular regions of protein/peptide aggregates [1-4]. The formation of specific protein aggregates, named amyloid fibrils, is considered a generic hallmark of these pathologies. Amyloid fibrils are ordered aggregates with a highly organized H-bond pattern, representing the most stable state that proteins can adopt [5]. It is nowadays accepted that the formation of abnormal oligomers during amyloid assembly pathway is at the basis of toxicity [6-8]. These species, often metastable, may disrupt cell membranes and eventually cause cell death by activating multiple unwanted cellular responses via mechanisms that are not yet well understood and need to be unraveled.

The self-assembly of Aβ peptide into fibrillar structures is closely related to the Alzheimer's disease (AD) development. The 40 residues Aβ(1-40) peptide is in fact naturally occurring from the proteolitic cleavage of the amyloid precursor protein (APP) [9,10] and it is the most abundant Aβ species in human brain. However, such fragment can also undergo an aggregation process and, in the aggregated form, it is found to be one of the major components of insoluble plaques detected in brains of AD patients [11].

The Aβ(1-40) peptide in solution is unstructured [12] and exists as an ensemble of rapidly converting, nearly isoenergetic, conformations whose population is dependent on the physico-chemical properties of the solution [13]. Depending on solution conditions Aβ(1-40) can also form amlyloid fibrils *in vitro*, giving the opportunity for a more thorough investigation of the aggregation kinetics. In specific conditions, aggregation-prone conformations can be favored, causing the onset of supramolecular assemblies [12,14]. Several reports indicate that the *in vitro* Aβ(1-40) aggregation process proceeds via multiple pathways involving a number of intermediate species eventually leading to polymorphic structures [15-16]. Recently, a chemical kinetic based approach was proposed as a powerful tool for connecting the measurements of macroscopic observables to microscopic mechanisms for Aβ amyloid formation. Such an approach aims at gaining insights into the multiple events involved in the formation of such supramolecular assembly *via* a detailed estimation of the rate constants of the reactions that are in turn connected to specific mechanisms, e.g. primary nucleation and/or more complex autocatalytic processes [17-20]. In this way the isolation of single steps of the kinetics is favored, thus helping in the identification of potential aggregation-prone

conformations in the early stages of the process. The latter is one of the main challenges that need to be dealt with.

In this context the possibility of using small molecules to modulate the aggregation pathway and isolate the occurring species has recently been considered as a potential tool for therapeutics [17, 21-24]. Such molecules may reduce the production of oligomers or alter the balance of protein-environment interaction favoring supramolecular assembly thus increasing the clearance of reactive species (e.g. toxic oligomers). Such molecules can delay or stimulate the fibril formation, stabilize specific intermediate species or even disrupt the final aggregate [25-28]. Evidences of the occurrence of such events have driven an increasing interest towards the understanding of small molecule-peptide interaction [29-31]. In particular the role of specific residues in the peptide-molecule interactions and the possible changes in conformation upon interaction should be better clarified.

In the case of the Aβ peptide, it has been established that the hydrophobic core, consisting of residues 17–21 (Leu^{17}-Val^{18}-Phe^{19}-Phe^{20}-Ala^{21}), plays a key role in the interaction with small molecules influencing the fibrillation process. Masuda and co-workers [31] reported that the small molecule Curcumin can affect both Aβ(1-40) and Aβ(1-42) [22] amyloid fibril formation, with 12 and 17-21 residues of the peptide being mainly involved in the interaction. Moreover, Tjernberg and co-workers [32] showed that the peptide fragment including residues 16-20 (Lys^{16}-Leu^{17}-Val^{18}-Phe^{19}-Phe^{20}) is the shortest one displaying a high binding capacity to the full length Aβ(1-40) peptide and the ability of inhibiting *in vitro* fibrils formation. Recently, Viet and co-workers [33] demonstrated that this fragment binds to residues near the N-terminal, Gly^{9} and His^{13}. For such kind of studies both experiments and simulations have been employed. Specifically, Molecular Dynamic (MD) has been recently employed in the emerging field of metallo-proteins and protein-metal interactions [34, 35]. In the case of the Aβ peptide, MD results have been employed not only to guide experiments, but have also been instrumental in designing potential Aβ aggregation inhibitors [36, 37].

We have recently reported that Thioflavin T (ThT), a fluorescent probe commonly used as a amyloid-specific dye, promotes Aβ(1-40) aggregation under near-physiological conditions [38]. In particular, the *in situ* presence of ThT resulted to be necessary to trigger the Aβ(1-40) aggregation process in quiescent

conditions [38]. As a consequence, ThT configures itself as a good model molecule for the investigation of molecule-induced modulation of the aggregation process, as it is simultaneously the target molecule and the tool to monitor the process. In the light of the specific ThT properties, we inferred that hydrophobic and electrostatic interactions between Aβ and ThT can potentially be at the basis of the enhanced Aβ(1-40) aggregation propensity in the presence of the dye. However, the mechanism of action shifting the protein ensemble towards a more aggregation-prone state remains to be clarified as well as the induced aggregation pathways. Either a specific stabilization of aggregation prone conformations, with the dye acting as a template, or a purely unspecific steric effect can be hypothesized. The occurrence of both mechanisms has been reported with reference to the behaviors of certain small organic molecules [39-41].

Here we present a combined experimental and MD simulation study of the microscopic mechanisms underlying Aβ(1-40)-ThT interaction. Experiments highlight different aspects and the intrinsic complexity of observed supramolecular assembly. In particular combined high-resolution microscopy and spectroscopy techniques revealed the inherent presence of multiple assembly mechanisms triggered by the ThT presence in solution, which give rise to aggregates with different properties. MD simulations allow to single out the potential role of specific peptide residues in the interaction with the dye. Moreover, it is possible to identify peculiar structural arrangements and geometrical properties of the ThT-induced conformation of Aβ(1-40) leading to the onset of the aggregation process.

Methods

Sample preparation. Thioflavin T (ThT) dye was purchased from Sigma Aldrich and used without further purification. Aβ(1-40) was purchased from Biopeptide. According to a slightly modified Fezoui protocol [42] the peptide was dissolved in a 2 mM NaOH aqueous solution (pH 10), sonicated for 30 min in a ice-water bath, and freeze-dried before being stored at -80 °C. This preliminary procedure leads to the disaggregation of the peptide. For the experiments, the peptide was dissolved in 50 mM sodium phosphate buffer, pH 7.4, with or without ThT, and filtered through 0.20 μm filters. Both the disaggregation and dissolution procedures were accomplished in a cold room in order to avoid seed formation. Aβ(1-40) and dye

concentrations were estimated by means of absorbance measurements using a molar extinction coefficient of 1390 M^{-1} cm^{-1} at 276 nm and 36000 M^{-1} cm^{-1} at 412 nm, respectively.

Rayleigh Scattering and ThT Fluorescence measurements. Fluorescence and Rayleigh scattering measurements were carried out simultaneously during the incubation of the sample at the desired temperature. Measurement were acquired every minute in standard right-angle geometry on a 0.5 × 1.0 cm PMMA UV-cuvette (BRAND) under excitation at 435 nm using a fluorescence system (ACTON Instruments) equipped with a PIXIS charge coupled device as a detector. A Xenon lamp (75 W) was used as a light source. Rayleigh scattering signal at 90° was measured as the maximum of the elastic peaks of excitation light (435 nm). Complete fluorescence intensity spectrum was measured at each time in order to highlight (if any) changes in its shape. Within the experimental error ThT emission measured in present experimental conditions did not show unsought peak deformation. Data were corrected for possible lamp intensity fluctuations. All the reported aggregation kinetics were measured in quiescent conditions and experiments were performed in triplicate showing a high degree of reproducibility.

Transmission Electron Microscopy. Grids were prepared as described by Foderà and co-workers [43]. Briefly, 5 µL of the sample were loaded onto copper 400 mesh grids (Agar Scientific, Stansted, UK) coated with Formvar and carbon film. After 60 s, 10 µL of distilled water was added and excess water was removed. Subsequently, 10 µL of 2% (w/v) uranyl acetate (Agar Scientific) was placed on the grid and left for 30 s. Finally, 2x10 µL distilled water were added and again excess water removed. The grid was then left to dry. The same procedure was used for the two samples under investigation. Images were collected using a CM100 transmission electron microscope operating at an acceleration voltage in the range of 40-100 kV.

Foster Recovery After Photobleaching (FRAP) measurements. Aβ(1-40) samples after incubation at 41 °C were cooled down in an ice-water bath before carrying out the measurements. Drops (10 µl) were placed in chambered cover-glass and imaged using a Leica RCS SP5 confocal laser scanning microscope with a 63× oil objective numerical aperture (NA) = 1.4 (Leica Microsystems, Germany). Confocal experiments were performed using the available FRAP wizard of the LEICA control software.

Circular Dichroism (CD) measurements. Measurements in the Far-UV region were carried out on a Jasco J-715 spectropolarimeter, equipped with a Jasco PCT 348 WI temperature controller. Sample cell paths were 0.5 mm. Spectra were acquired using a scan speed of 50 nm/min, data pitch of 0.1 nm, response of 2 s, number of accumulations 4. Measurements on thermally treated samples were carried out just after cooling down in an ice-water bath.

Classical Molecular Dynamics. Classical MD simulations of the Aβ(1-40) peptide in interaction with 5 ThT molecules in water were performed employing the GROMACS package [44]. The systems are simulated in the NpT-*ensemble*, using the GROMOS53A6 force field [45] which was recently tested to properly work for Aβ(1-40) in the work of Gerben et al. [46]. The temperature is held fixed at 300 K using the v-rescale thermostat [47] with a coupling time of 0.1 ps. The pressure is kept constant at the reference pressure of 1 bar with a coupling time of 1 ps and an isothermal compressibility of $4.5 \cdot 10^{-5}$ bar^{-1}, exploiting the features of the Berendsen barostat [48]. The single point charge (SPC) model is used for water molecules. The ThT force field was computed with the help of the Automated Topology Builder and Repository [49] and implemented in GROMOS53A6.

The number of water molecules (more than 122.000) in the simulation box[1] is such that the Aβ(1-40) concentration is about 400 μM. An appropriate number of counter-ions (Na^+ or Cl^-) is added in order to have a wholly neutral system. MD simulations are performed at neutral pH. In other words the protonation state of the peptide was chosen so as to have N-terminus, arginine and lysine protonated and positively charged, while C-terminus, glutamic and aspartic acid are deprotonated and negatively charged, a choice corresponding to the expected protonation state of free amino acids at neutral pH.

Periodic boundary conditions are used throughout the simulation and Particle Mesh Ewald algorithm is employed to deal with the long-range Coulomb interactions [50]. The integration time step is 2 fs. A non-bond pair list cutoff of 1.4 nm was used, and the pair list was updated every ten steps. For each system in study we have collected trajectories as long as 90 ns.

The simulation strategy we followed is the same as in ref. [37]. The relevant structural and dynamical

1 The volume of the cubic simulation box is $15.4^3 \approx 3652$ nm^3.

information about the simulated systems are extracted only using the last 60 ns of the collected trajectories, in order to perform the analysis employing sufficiently well equilibrated system configurations. We will also occasionally discuss the transient behavior represented by the first 30 ns from which one can extract useful information on how the systems approach equilibrium. The structural analysis of the collected configurations was carried out using some of the available GROMACS tools and a number of "home-made" codes expressly written for the purposes of the present investigation.

Results and Discussion

Effect of temperature on Aβ(1-40) aggregation kinetics. In Figure 1A we report the time evolution of Rayleigh scattering intensity growth as a function of time for three identical 120 μM Aβ (1-40) samples containing 33 μM ThT and incubated at 37 °C (cyan circles), 41 °C (blue plus) and 45 °C (dark pink cross). In Figure 1B we show ThT fluorescence intensity kinetics simultaneously acquired during the scattering measurements. Rayleigh scattering intensity provides information about the average size of particles in solution and gives qualitative information about the overall aggregation process [51].

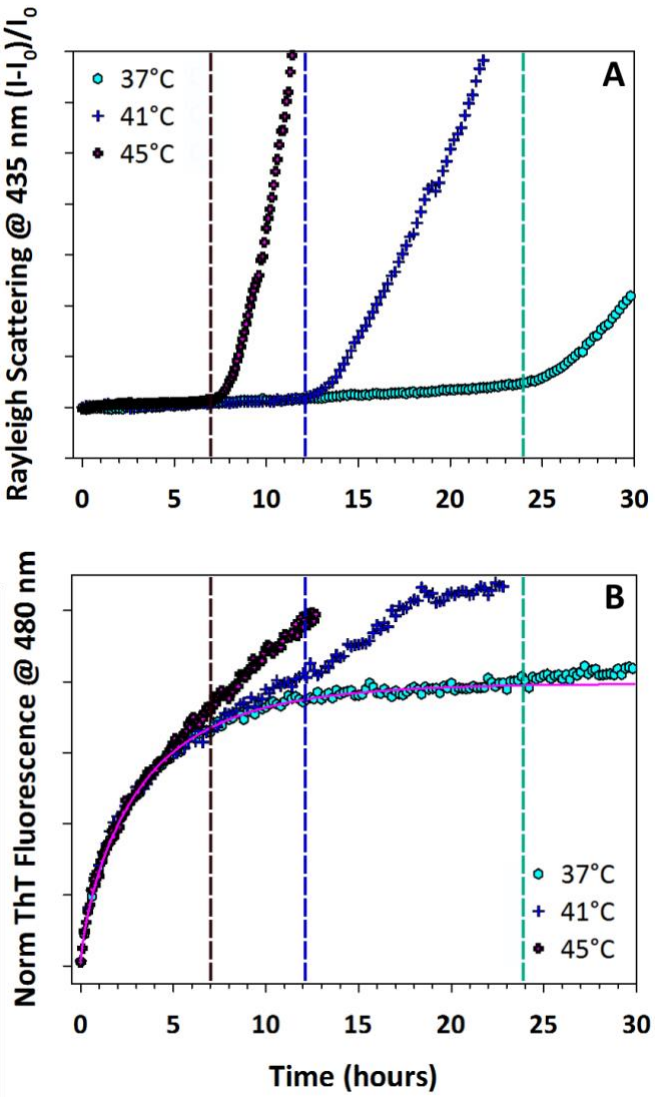

Figure 1

ThT fluorescence kinetics gives information on the presence/growth of amyloid-like structures. Data are normalized to the ThT intensity value after 3 hours of incubation. The direct comparison among absolute values of fluorescence intensity at the different temperatures is, in fact, not possible due to the dependence of the quantum yield on temperature [52]. However, comparison of the temporal profiles of fluorescence signals during isothermal experiments provides significant information about the activation times and growth rates of the occurring processes.

As it can be seen, scattering signal shows a two-step kinetics with a high degree of reproducibility: a lag-phase in which the signal slowly increases almost linearly, and a subsequent slope change resulting in an

abrupt growth. These observations are in line with what previously observed: in the presence of ThT in analogous conditions [38] aggregation is observed, while no scattering growth (massive aggregation) was observed in the absence of ThT. Dashed lines in Figure 1A indicate the duration, t_0, of the first part of the lag-phase. The same lines are reported in Figure 1B as a reference. The duration of the lag-phase t_0 and the slope of the signal growth in the second phase are critically dependent on temperature, being the whole process faster at higher temperatures. ThT fluorescence kinetics in Figure 1B shows an almost monotonic growth. However, a closer inspection of the data may reveal a first concave growth for $t<t_0$ (to the left of the dashed lines) and a second almost linear growth. The occurrence of the second phase and its slope strongly depend on temperature. The kinetic ThT fluorescence profile in the first phase overlaps for ~6-7 hours without showing any significant temperature dependence. From this observation, it is possible to infer that, in the observed conditions, and at least in the early stages, ThT signal growth is characterized by the same kinetic profile in experiments at different temperature. Only the signal of the sample incubated at 37 °C reaches a plateau before the onset of the second phase, which is clearly detected by light scattering (Figure 1A). Rayleigh Scattering and ThT fluorescence signals show different temporal evolution, the first being characterized by a marked biphasic behavior with a steep increase in the second phase, while the second one starts with a monotonic growth and undergoes a less prominent change in the second phase.

The simultaneous analysis of ThT fluorescence kinetics with other observables may help revealing multiple facets of the same process. Data in fig. 1 show lack of correlation between scattering and ThT fluorescence kinetics acquired simultaneously, highlighting the possible presence of different interconnected aggregation pathways, likely characterized by different intermediate species with different affinities to the dye [53].

The first concave growth in the kinetics at 37 °C can be fitted using a stretched exponential function $Y=1-\exp\left[-(\beta t)^{\gamma}\right]$ with β~0.37 sec^{-1}, γ~0.72 (pink line in Figure 1B). Stretched exponential function can be used to provide a description of phenomena characterised by the presence of a highly heterogeneous sequence of events or species regulated by a distribution of activation energies. Importantly, such a fitting procedure does not imply specific models based on molecular mechanisms. The stretched exponential function ($\gamma<1$) also represents a particular case (with $m=1$) of the so-called “autocatalytic model” that has

been developed for assembly processes in which an array surface catalyzes the rate-determining formation of a critical "nucleus" of *m* units [54]. The finding $\gamma<1$ further corroborates the presence of multiple pathways already indicated by the lack of correlation between ThT and scattering data. Concave ThT fluorescence growth was previously observed in Aβ supramolecular assembly process characterized by a nucleation process occurring in presence of seeds [20, 55, 56]. This kinetic profile usually reflects the occurrence of heterogeneous nucleation mechanisms along aggregation pathways [57].

Data in fig. 1A and indicate the presence of a series of interconnected mechanisms (Figure 1). The initial increase of the ThT signal does not depend on dye concentration [38] and shows a weak dependence on temperature (Figure 1B).

Effect of ThT on Aβ(1-40) initial and intermediate states during aggregation. To gain further insights into the early phases of the process, we analyzed the initial peptide state (before thermal treatment, with and without ThT) and the species formed at t_0 (dotted line in Figure 1) by means of imaging techniques.

In Figure 2, representative transmission electron microscopy (TEM) measurements are reported for 150 μM Aβ samples in the presence of 30 μM ThT (panels A, B) and in the absence of ThT (panels C, D) before incubation. The two samples were freshly prepared using identical protocols and then dried on the sample holder (see Materials and Methods).

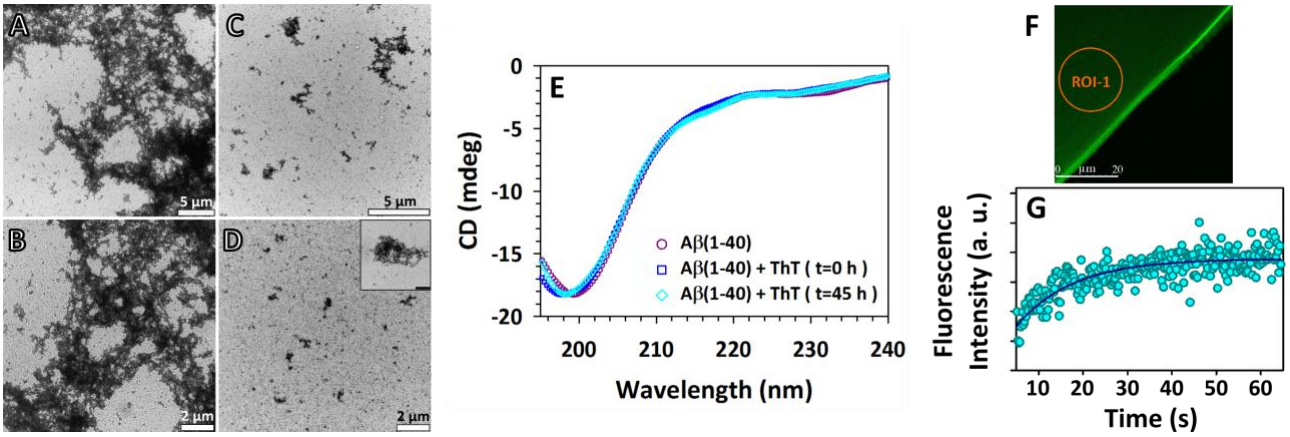

Figure 2

Large quantities of aggregates are found in the samples where ThT is present (Figure 2A and 2B), in particular a network of tiny aggregates possibly formed by elongated substructures is observed. On the contrary, samples where ThT is not present show very few aggregates of smaller size and with lower level of organization (Figure 2C and 2D). Obviously, these measurements do not reflect actual conditions at the first stage of the kinetics, since samples underwent (identical) drying procedure before imaging, possibly favoring aggregation. However, it is worth noticing that, since the preparation protocol for the two samples is identical, any difference between them can be related to nothing else than their intrinsic nature. Figures 2 (panels A to D) reveal for Aβ(1-40) an increased tendency to aggregate when ThT is present, even at room temperature. These measurements indicate that changes induced by the presence of ThT in solution are effective right after the sample preparation and before thermal treatment.

In Figure 2E FAR-UV CD spectra of Aβ(1-40) samples in the presence and in the absence of ThT are reported together with the spectrum of the sample after 45 hours of thermal treatment at 41 °C. Importantly, no significant differences are found among spectra. CD measurements in Figure 2E indicates that even after 45 hours of incubation, i.e. when large aggregates positive to ThT (see e.g. fibrillar structures imaged in ref. [38]) are present, the CD spectrum does not display significant changes with respect to the one of the protein in the initial state before incubation. This observation can be explained noting that only a small fraction of the sample is converted into fibrils, leaving a significant part of the molecule with a nearly unchanged secondary structure. In this case, as also commented by Arosio et al. [58], the resolution of CD technique may not allow the detection of small fractions of aggregates/peptides with a modified secondary structure.

To further investigate the initial phase of the aggregation process, we then analyzed, as an example, an Aβ(1-40) sample after 6 hours of incubation at 41 °C in the presence of ThT, that corresponds to an advanced stage of the initial growth phase whose end is indicated with the blue dashed line in Figure 1A. This point of the kinetics corresponds to the end of the common growth of ThT fluorescence kinetics measured at the different temperatures (Figure 1B). We performed single color confocal microscopy measurements whose results are shown in Figure 2F. The uniform green signal takes into account ThT fluorescence when the dye interacts with protein aggregates whose size is below the instrumental resolution (~200 nm). It is possible to quantify

the size of these aggregates using Foster Recovery After Photo-bleaching (FRAP) technique. Several FRAP experiments were performed in different areas of the samples showing a homogeneous presence in solution of small aggregates bound to ThT. In Figure 2G a typical profile of fluorescence recovery curve from a circular area of 10 μm-radius is reported. According to such fluorescence recovery, standard analysis using the Kapitza model [59] allows one to calculate a diffusion coefficient D = 29 $\mu m^2/s$. Similar measurements on different solution areas using bleaching regions (with radius from 5 to 30 μm) revealed the presence in solution of small aggregates (bound to ThT) with hydrodynamic radius ranging between 5 nm and 25 nm. In contrast with other standard techniques (e.g. light scattering or bulk ThT fluorescence), these measurements allow one to isolate the contribution of the population of molecules that bind to ThT and contribute to its fluorescence enhancement, also determining their size. These aggregates of fibrillar nature also contribute to the first scattering growth observed in Figure 1 and, importantly, they are uniformly distributed in the whole sample (within instrumental resolution). These structures can either 1) be seeds for further aggregation, 2) represent propagons [58, 57] that may further interact with non-fluorescent species or 3) be involved in an independent assembly pathway.

Effect of Aβ concentration on the aggregation kinetics. The study of Aβ(1-40) assembly kinetics as a function of concentration gives information on the underlying aggregation mechanisms. It is informative about the possible presence of both homogeneous and/or heterogeneous nucleation pathways [17-20, 60].

Figure 3 shows the time evolution of Rayleigh scattering intensity (A) and ThT fluorescence intensity (B), acquired for five Aβ(1-40) samples with peptide concentration ranging between 25 μM and 150 μM, containing a constant concentration of ThT (28 μM), during isothermal incubation at 41 °C. The insets in panel (A) and (B) report respectively Rayleigh scattering and ThT fluorescence intensity as a function of time for three Aβ(1-40) samples incubated at 37 °C at a peptide concentration of 50 μM, 115 μM and 160 μM. As previously reported [38], in these conditions and in the absence of ThT, no aggregation is observed as monitored by Rayleigh scattering.

Data in Figure 3A clearly show a biphasic behavior analogous to the one reported in Figure 1A. It is noticeable that really small variations are observed in the duration of the first phase (t_0) as a function of

monomer concentration. In Figure 3B ThT fluorescence growth is not observed for samples at peptide concentration lower than 65 μM. In these samples Rayleigh scattering growth is observed only after t_0, indicating the occurrence of massive aggregation. For sample with peptide concentrations higher than 65 μM, ThT fluorescence intensity increases. In particular, the monotonic concave growth of the kinetics is larger at higher peptide concentration. This shows that, in these conditions, peptide molecules interact with the dye, resulting in an increased quantum yield since the very early stages. This last fact indicates that the protein-solvent-dye balance of different interactions is also regulated by peptide concentration, probably affecting peptide 3D organization via long-range forces.

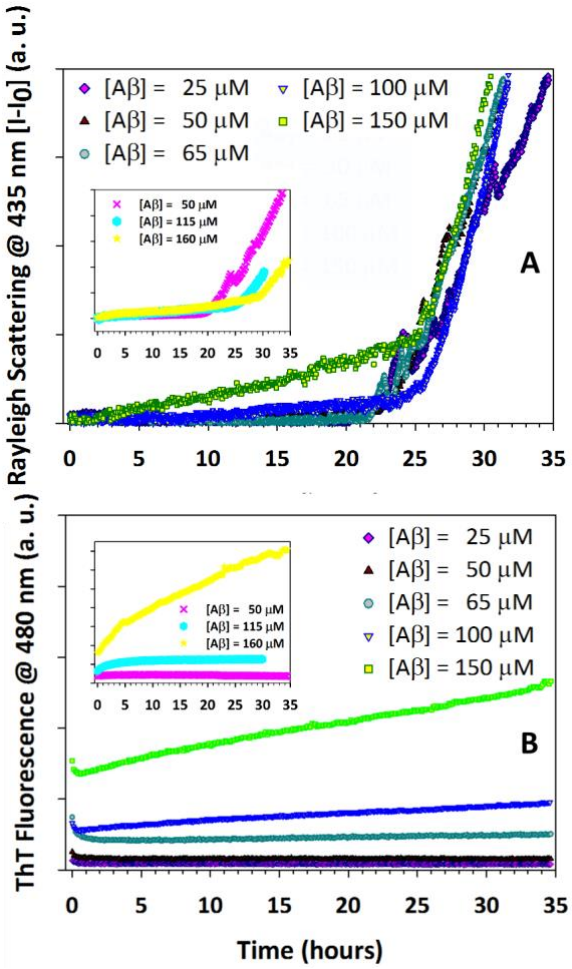

Figure 3

In samples at lower peptide concentration, scattering intensity in Figure 3A shows a biphasic behavior with a no significant signal increase in the first phase. Similarly in these samples ThT fluorescence intensity growth is not observed (Figure 3B).

In samples at higher peptide concentration, the ThT fluorescence intensity growth is paralleled by scattering increase in the first step, whose slope depends on concentration.

This phenomenon is more evident for the 150 μM sample when the first 25 hours are examined, thus suggesting that the scattering species during this phase are of amyloid-like origin.

A closer inspection shows that the duration of the first phase in Rayleigh scattering growth remains unvaried when protein concentration is increased from 25 μM to 65μM (i.e. when ThT fluorescence signal growth is not significant), at higher concentration a really small variation of t_0 is detected. Specifically, in samples at peptide concentration of 100μM and 150μM the duration of the first phase increases by about 3 hours with respect to the lower ones. In Fig.3 inset analogous measurements obtained at 37°C. As it is evident the whole process speeds up when the peptide concentration is decreased, being the first phase shorter at lower peptide concentration.

This atypical peptide concentration dependence together with the high reproducibility of the observed kinetics (generally observed in the case of templated processes) indicates a major role of ThT in the aggregation process. The process seems to involve multiple reacting species in different stages whose equilibrium depends on relative concentration of reagents, which vary at each time point and that are differently regulated by external factors (e.g. temperature). At lower Aβ concentration, i.e. in conditions where ThT fluorescence intensity growth is not observed, large aggregates formation occurs, indicating the formation of aggregates that do not bind ThT. At higher concentration ThT interacts with Aβ(1-40) molecules since the very first stage of aggregation, leading to ThT- positive aggregates.

Moreover, data in Figure 3, in combination with previously reported experiments (see Figure 2 in [38]), suggest that peptide-ThT interaction dominates the aggregation reaction in such a way that the rate constants

of the processes (ThT positive and massive aggregation) depend on the ratio between dye and peptide concentrations but that absolute peptide concentration also plays a significant role in regulating assembly mechanisms.

Interaction of the dye with the peptide may lead to the formation of activated species, which act as a rate limiting step for the massive aggregation revealed by Rayleigh scattering. Indeed, as we shown in ref 38, at constant peptide concentration, the duration of the lag-phase depends on ThT concentration. On the contrary, Figure 3 shows that, fixing the ThT concentration, the duration of the lag-phase does not depend on Aβ concentration as long as the ThT fluorescence signal does not increase. Moreover, when an increment in ThT fluorescence intensity is monitored, the duration of the lag-phase increases as a function of peptide concentration. This indicates that the formation of ThT-positive species acts in competition with that of activated species

Self-assembly process appear to be modulated by ThT-mediated interactions. If the reaction would have been regulated only by pure peptide-peptide interaction, the aggregation process would have occurred only via stochastic nucleation mechanisms (i.e. low degree of reproducibility [61]) with a strong dependence of the lag-phase on the peptide concentration [62, 63]. On the contrary, we found that ThT presence in solution clearly alters the balance between monomer-oligomers-fibrils populations (Figure 2A-D), so that classical scaling laws for aggregation process are not followed. It is anyway worth noting that the growth of aggregates able to bind the dye depends on the peptide concentration, and that, at higher peptide concentration, these structures undergo a further reorganization leading to the concave profile typical of assembly kinetics regulated by complex nucleation mechanisms (Figure 3).

In summary, results reported till now suggest the coexistence of at least two distinct aggregation pathways. Aggregates able to bind to ThT ("ThT-positive" aggregates) are formed in the early phase and their number increases as the peptide concentration rises. Furthermore, Rayleigh scattering data reveal that the abrupt aggregates growth, observed in the second part of the process ($t>t_0$), occurs only if the ThT is present in solution [38] and may occur even in the absence of a ThT fluorescence intensity growth. That is, the formation of small aggregates that bind to ThT is not directly linked to the occurrence of the massive

aggregation at $t>t_0$, but the presence of the dye is a *conditio sine qua non* for the activation of massive aggregation. Both processes are triggered by ThT though by different mechanisms and different peptide concentration-dependence. Moreover, the early formation of ThT-positive species may act in competition with massive aggregation observed at longer time. This effect is emphasized in experiments at 37 °C (Figure 3, insets). At increasing peptide concentration, an enhanced population of ThT-positive aggregates is initially formed (Figure 3) probably having as a direct effect the depletion of peptide molecules free to contribute to massive aggregation for $t>t_0$. This in turn determines the apparent "reverse" dependence on concentration of t_0 (Figure 3) observed at 37 °C and barely visible at higher temperatures. Importantly, since such an effect is more evident at lower temperature, we can also conclude that the two aggregation pathways have different temperature dependence. Regarding the activation of the massive aggregation, we can infer that ThT presence templates the formation and the enrichment of a population of a reactive species during the lag-phase [64]. These species may constitute critical nuclei for further nucleation mechanisms.

Alternatively, the observed templated process could resemble the aggregation mechanisms followed by an ensemble of proteins in the presence of preformed seeds [55, 56]. This last hypothesis supported by the absence of clear peptide concentration dependence for this process, while a strong ThT concentration dependence is observed [38].

Molecular Dynamics Simulation and Aβ(1-40)-ThT interaction. In the previous section we presented evidences of the direct effect of ThT on the monomeric peptide and, as a consequence, on the aggregation kinetics. Given the complex interactions highlighted by experimental data, it would be an important piece of information to obtain insights into the way the dye interacts with a single peptide triggering the aggregation process. To this purpose we performed MD simulations, that allows the investigation at atomistic level of the mechanisms involved in the interaction between Aβ(1-40) peptide and ThT molecules. MD simulation are aimed at identifying possible ThT binding sites, getting indications on most stable Aβ(1-40) conformations

and on their potential reactivity. As a consequence, the interest is focused on the interaction of ThT molecules with one Aβ peptide.

We performed classical MD simulations of a model system where one Aβ(1-40) peptide is dissolved in water together with 5 ThT molecules. The rationale for this choice is to monitor the behavior of a system where a sufficiently high number of ThT molecules are in position of interacting with the Aβ(1-40) peptide thus facilitating the search for possible Aβ(1-40)-ThT interaction sites and highlighting any ThT-induced change in the Aβ(1-40) conformation.

Starting from the Aβ(1-40) NMR structure ID:1IYT [65] we analyzed the effect of the presence of 5 ThT molecules on the peptide structure and conformation during the MD simulation time, using different structural indicators. Data were compared to the case of Aβ(1-40) peptide in water in the absence of ThT.

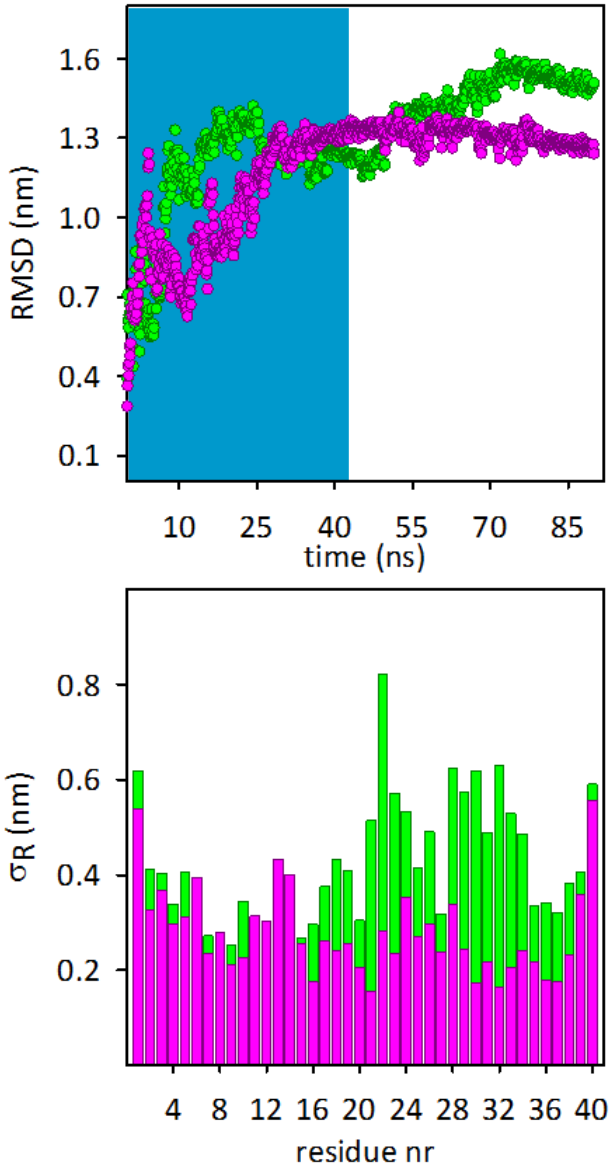

Figure 4

We report in Figure 4A the Root Mean Square Displacement (RMSD) of the peptide [66] as a function of time referred to only the peptide backbone atoms of the Aβ(1-40) (green points) and Aβ(1-40)-ThT (magenta points) systems along the 90 ns of the NpT simulation. The time behavior of RMSD was computed by means of the g_rms [66] GROMACS tool, using as a reference configuration the PDB structure from which MD simulations were started.

As it can be seen in the region between 30 ns and 90 ns, the value of RMSD as a function of time is quite stable in the presence of ThT (magenta) while in the absence of dye molecules (green) it reaches a plateau

only in the last 20 ns (Figure 4A). Moreover, in the first 30 ns (dark cyan area), the two systems display quite a different approach to equilibrium. In the absence of ThT the RMSD of the Aβ(1-40) system (green) moves rapidly to a plateau, while the Aβ(1-40)-ThT system (magenta) gradually approaches it. A comparison of the mobility of the two systems can be performed in terms of the quantity

$$\sigma_R = \left[\frac{1}{T} \sum_t \frac{1}{N_R} \sum_j | r_j(t) - \langle r_j \rangle |^2 \right]^{1/2} \quad (1)$$

where T is the length of the MD trajectory, $\{r_j(t), j=1,..., N_R\}$, are the positions of the N_R atoms belonging to the residue R and $<r_j>$ represents the average position of the j-th residue atom along the trajectory. For the computation of this quantity only the last 60 ns of the simulation was used. The behavior of σ_R as a function of the aminoacid residue position for the two systems of interest is displayed in Figure 4B. The mobility σ_R is computed using the g_rmsf GROMACS routine.

The kind of values taken by σ_R at the amino acid residue position suggests that interactions with ThT force constraints that reduce the size of the basin of the peptide accessible conformations. The 1-16 region doesn't show significant mobility differences, that are instead well visible in the 17-38 region. This region includes the central hydrophobic cluster Leu^{17}-Val^{18}-Phe^{19}-Phe^{20}-Ala^{21} known to form the core of the minimum fibril forming sequence [67] that is considered crucial in the aggregation process. Indeed, planar aromatic interactions involving the two Phe residues were proposed to stabilize the fibrillar structure and to determine the main structure of the amyloid fibrils [68].

These modifications can be ascribed to the direct interaction of ThT molecules with specific Aβ(1-40) residues. To verify such hypothesis, we measured the time evolution of the distance between the Aβ peptide and each one of the 5 ThT molecules. In Figure 5, for each ThT molecule, the occurrence of an event where a ThT molecule approaches a specific Aβ(1-40) residue is reported as a function of the simulation time.

Specifically, a given symbol is drawn in the plot if the center of mass of the *n*-th ThT molecule is found within 8 Å from anyone of the Aβ(1-40) backbone atoms[2].

As shown in Figure 5 all the five ThT molecules approach the peptide. However, the time of permanence in the peptide vicinity is quite different. In particular both ThT nr. 1 and nr. 4 approach the peptide for a very short time, the former ThT nr. 1 at the end of the simulation trajectory and ThT nr. 4 in the interval 36-39 ns.

ThT molecule nr. 2, instead, comes close to the Aβ(1-40) peptide after about 48 ns and remains in its vicinity until the end of the simulation. Specifically, it interacts with the residues located at the two extremes of the 3-26 fragment. It is interesting to note that ThT nr. 2 interacts with an unstructured region by acting as a "lock" that imposes stable hairpin like structure. ThT molecule nr. 3 approaches the peptide backbone (fragment 5-25) immediately after the simulation starting and remains in this position for the whole simulation.

As it is clear from Figure 5, both ThT nr. 2 and nr. 3 are found to predominantly interact with aromatic residues. ThT nr. 2 interacts with the peptide in the region 3-6 namely with the sequence Glu-Phe-Arg-His, and 24-27 i.e. Val-Gly-Ser-Asn while ThT nr. 3 interacts very stably along the whole simulation time with the peptide in regions 10-11 (Tyr-Glu) and 19-21 (Phe-Phe-Ala), forcing these last residues in a more rigid conformation as shown in Figure 4B. Finally ThT molecule nr. 5 is found in the vicinity of the peptide (28-40 region) in the last 14 ns close to the β-sheet structure. It cannot be excluded that this ThT molecule may possibly have a role in the peptide-peptide interaction. Indeed, the vicinity of the molecule to the β-sheet structure could favor intermolecular interactions [70] able to block the ThT molecule in between two peptide molecules.

2 The 8 Å-limit is chosen to be slightly larger than the sum of the van der Waals radius of Aβ(1-40) and the *n*-ThT molecule.

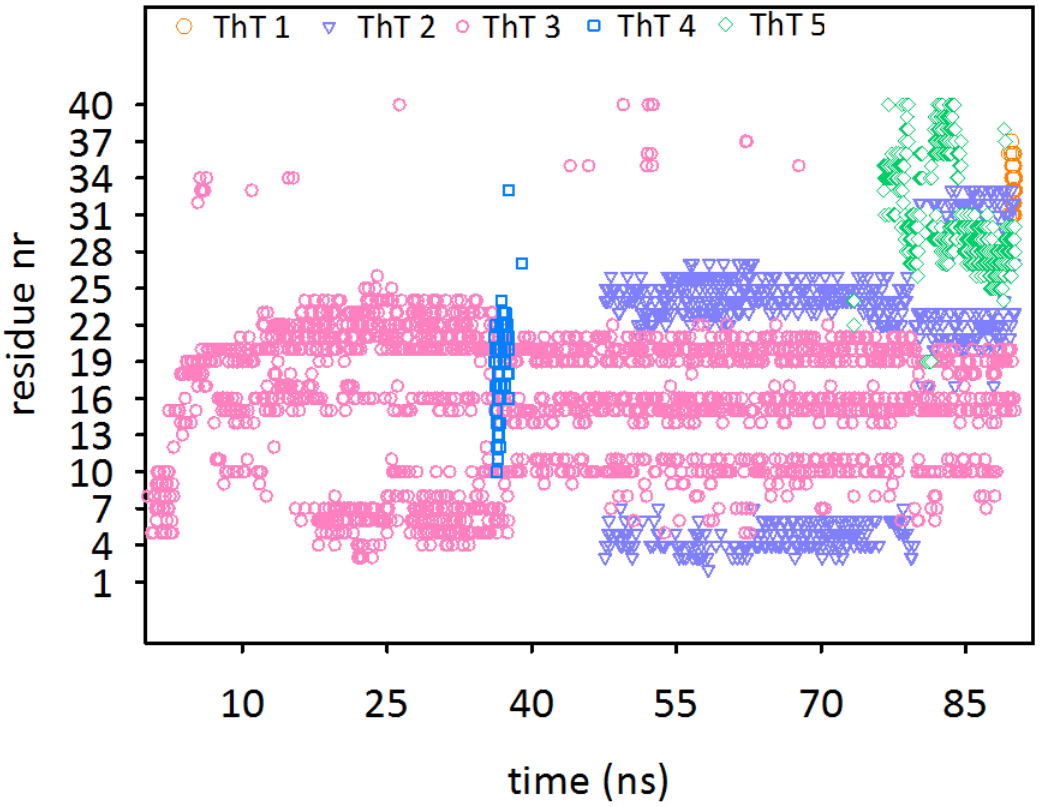

Figure 5

We also monitored secondary structure evolution during the simulation using a protocol for the definition of secondary structure of proteins (DSSP) previously proposed in [69] and implemented in GROMACS in the do_dssp tool. In Figure 6 we show DSSP results as a function of the simulation time for the Aβ(1-40) peptide both in the absence (panel A) and in the presence (panel B) of ThT. Above each DSSP panel, we draw the photograms showing the most representative tridimensional structures of the cluster of configurations encountered every 10 ns [3].

3 The most representative structure of the cluster is computed by using the g_cluster GROMACS' routine and it is the centroid of the most populated cluster retrieved for each 10 ns time interval.

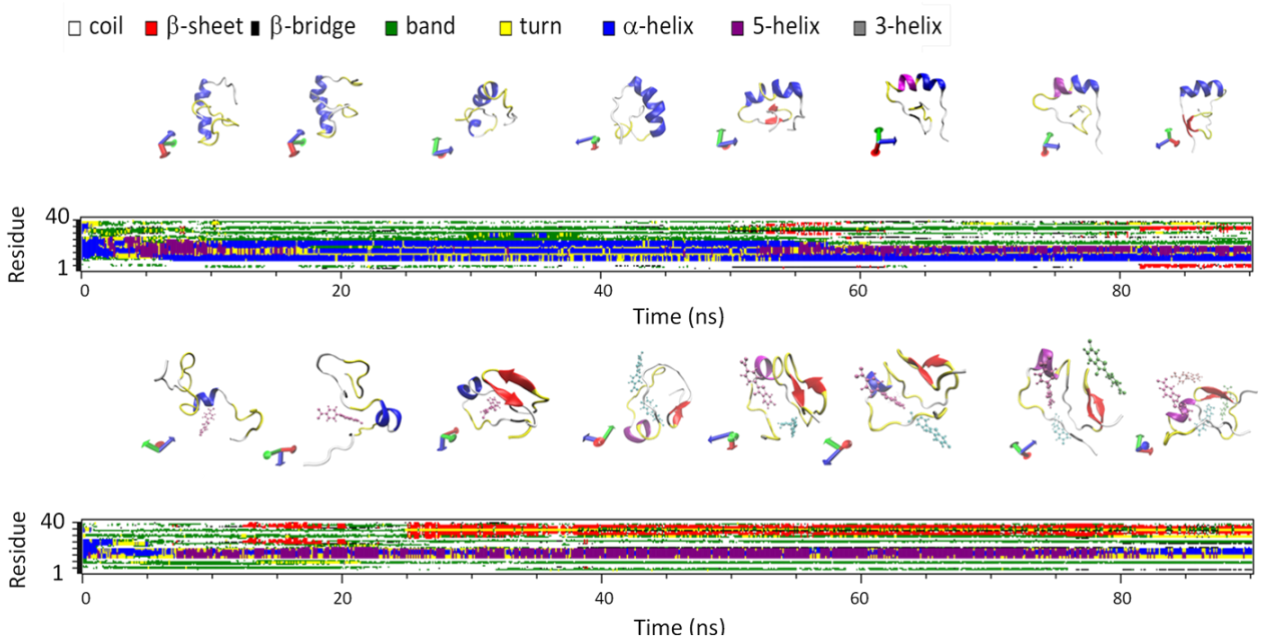

Figure 6

Looking atthe Aβ(1-40)-ThT system, one notices that the α-helix structure (blue) is completely lost after few ns. At the same time, β-sheet (red) and turn (yellow) structures in the 28-38 segment, together with a 13-20 segment of 5-helix, appear and remain almost stable for the whole simulation time. We report in Table 1 the relative content of secondary structure as computed along the final 60 ns. It is worth mentioning here that the influence of ligands on the Aβ(1-40) aggregation propensity relies on their ability of altering the peptide secondary structure organization. As an example, ligands able to increase Aβ helix stability are found to reduce fibrils formation, whereas compounds with no effects on secondary structure do not seem to affect fibril formation [37, 71].

	Coil	β-sheet	β-bridge	bend	Turn	α-helix	5-helix
Aβ	39%	2%	2%	19%	7%	23%	8%
Aβ-ThT	42%	10%	3%	20%	7%	4%	13%

Table 1

The ThT-peptide interaction is found to "lock" the peptide in a closed chain conformation where the hydrophobic region 28-38 is forced to form a short β-sheet that may act as a reactive site for peptides intermolecular interactions. In fact, looking at Figures 5 and 6, it can be noticed that, when ThT nr. 3 starts interacting stably with Tyr10 and Phe19, Aβ(1-40) takes a β-sheet structure in the 28-38 region and does not lose this structure irrespective of how many other ThT molecules approach the peptide. The observed differences of the folding of the two Aβ(1-40) systems, with and without ThT molecues, together with the close interaction of ThT nr. 2 and nr. 3 stabilizing an extended β-sheets structure in the first steps of the simulation, represent a proof on the role of the dye in controlling the secondary structure of the peptide, likely enhancing the overall aggregation propensity of the peptide ensemble. It is worth noting that, at the end of the simulation, ThT nr. 5 and, though for a reduced time, also ThT nr. 1 approach the peptide exactly in the β-sheet region, neither interfering with ThT nr. 3 nor with the stability of the 28-38 secondary structure.

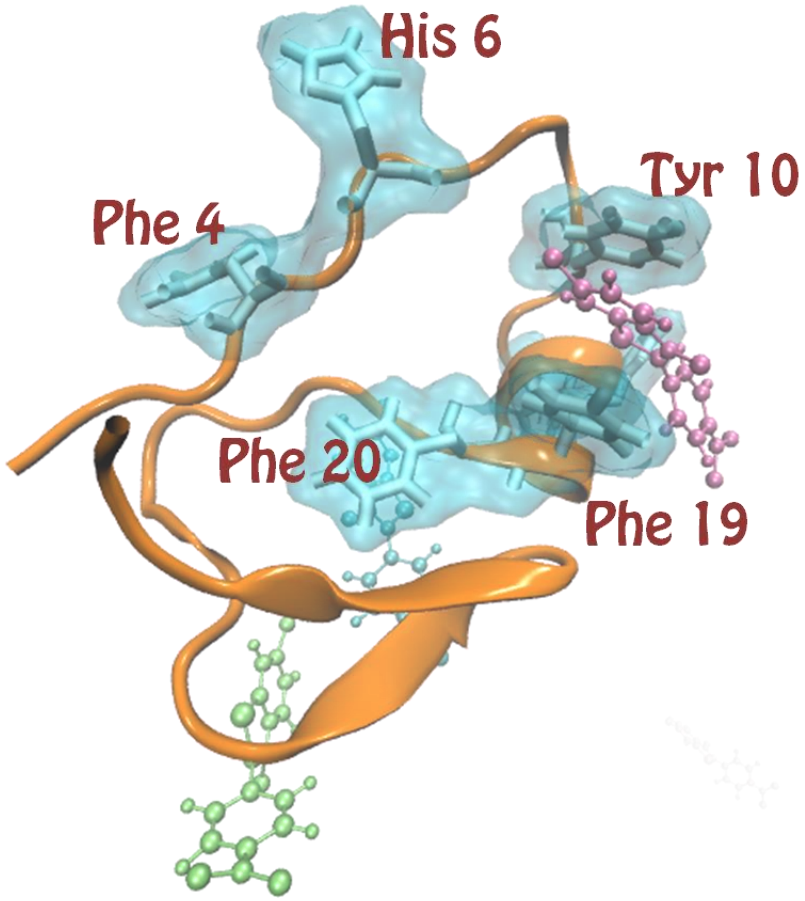

Figure 7

A representative structure of the last 10 ns of simulation is reported in Figure 7 where three ThT molecules are visible. The two aromatic rings in ThT nr. 3 are packed in between the aromatic rings of Tyr10 and Phe19. This configuration leads to the critical exposure of other aromatic residues that may take part in supramolecular association.

Although it is evident that simulation conditions are rather far from the experimental ones, the data we have presented can elucidate the experimentally observed effects of ThT on the Aβ(1-40) stability. The "locked" ThT-induced conformation contains a short β-sheet in the hydrophobic region and its subsequent reduced mobility may indeed change the energetic equilibrium of the peptide ensemble. This can probably lead to favorable stacking interactions also due to the varied spatial organization of the aromatic residues in presence of the dye as well as to selected directionality and orientation of new intermolecular bonding. This would be

in agreement with the tendency to aggregation experimentally observed by TEM imaging even at room temperature (Figure 2) and the ability of ThT in inducing aggregation processes (Figure 1 and 3), otherwise not present in its absence [38]. Specifically, we can postulate that this "locked" conformation may favor intermolecular interaction both with "template" molecules and unstructured monomers giving rise to the two different aggregation pathways experimentally observed. In particular a direct interaction of such ThT-induced conformation could in principle give rise to the formation of the ThT-positive aggregates, while interaction of such state with unstructured monomers could be at the basis of the observed massive aggregation. Further mechanisms can be also supposed including the interaction of Aβ or "templated" Aβ with ThT clusters or micelles, which are not observed in the present simulations, but might be present in real solution conditions and contribute to some extent to aggregation.

According to the MD data, the [ThT]/[Aβ(1-40)] ratio needed to experimentally observe an overall secondary structure conversion in real sample should be extremely high. In the presented experimental conditions only a fraction of the Aβ(1-40) sample would be able to interact with ThT, so that the extent of the expected secondary structure changes cannot be appreciated by CD, being them within the experimental error.

.

Conclusions

We presented a thorough study on the interaction between Aβ(1-40) and ThT and the effect of the dye on the Aβ(1-40) conformation and aggregation propensity. Experimental data show that ThT presence triggers a complex aggregation pathway with multiple intermediate states whose equilibrium depend on peptide concentration, [ThT]/[Aβ(1-40)] ratio and temperature. We previously demonstrated that at constant peptide concentration ThT presence induces aggregation and that increasing ThT concentration causes the acceleration of aggregation kinetics without modifying aggregation kinetic profile [38]. In the same experimental conditions, but in the absence of ThT, Aβ(1-40) aggregation processes do not occur.

Data presented here unequivocally show that the aggregation process induced by ThT involves at least two association mechanisms. One responsible for the massive aggregation revealed by Rayleigh scattering, the second one hinted by an increase of ThT fluorescence signal as a function of time and a small increment in the Rayleigh scattering signal, during the lag-phase.

At low peptide concentration no ThT fluorescence signal growth is observed and supramolecular assembly leads to the formation of "ThT-negative" aggregates. In these conditions, a proper lag-phase in scattering intensity kinetics is observed with no growth until the second phase occurs. At higher peptide concentration two aggregation pathways are activated. In the first stage, aggregation leads to the formation of "ThT-positive" complexes with this process being paralleled by a scattering growth of small extent. An abrupt growth in the scattering signal is observed after this "modified" lag-phase. The "ThT-positive" aggregates formed in the first stage likely decrease the protein material available for massive aggregation. The reduction of available protein material leads to a decrease of the rate of growth of the second part of the scattering signal.

In these conditions, where ThT fluorescence growth is observed, the energy barriers regulating the aggregate growth appear to be low enough not to result in significant temperature dependence of fluorescence kinetics. This is true at least in the first stages of the measurements where the formation of uniformly distributed oligomers binding to ThT is detected. All experimental data, point toward a templated-effect induced by ThT that regulates a supramolecular assembly process in which only a small fraction of peptides changes its conformation which is then converted into fibrils.

MD simulations confirm that ThT may interact with a single Aβ peptide and allow identifying possible binding sites of ThT molecules along the peptide chain. We have been able to highlight in this way the existence of a novel ThT-induced Aβ(1-40) conformation characterized by an enhanced content of β-sheet structures and a pronounced conformational rigidity. We identify the specific Aβ(1-40) regions involved in the interaction as being the residues 3-6 10-11 19-21. All together our results show the ability of ThT in modulating the aggregation reaction of Aβ(1-40) and provide new insights into both the Aβ(1-40) aggregation propensity and the possibility of using ThT as small molecule for the modulation of inter-protein

interactions. Our study also poses new questions regarding the needs of developing new quantitative and label-free techniques for a reliable (i.e. unbiased) investigation of Aβ(1-40) aggregation processes.

Authors Contribution

All Authors conducted the research. MGDC, VV,VF, VM,ML contributed to the experimental design. VM and SM contributed to Molecular Dynamics Simulation. All authors contributed to the preparation of the manuscript.

Acknowledgments

V.F. acknowledges support from the FP7 Marie-Curie Actions Intra European Fellowship (IEF) for Career Development 2012-2014, project nr. 299385 ‘‘FibCat’’ (University of Copenhagen). This work was partly financially supported by a national project (PRIN 2008) of the Italian Ministry of University and Research. We acknowledge the Core Facility for Integrated Microscopy, Faculty of Health and Medical Sciences, University of Copenhagen where the TEM measurements were performed. We thank Dr. Bente Vestergaard, Prof. Giancarlo Rossi, and the members of the Molecular Biophysics and Soft Matter group (http://fisicaechimica.unipa.it/biophysmol/people.htm/) at the University of Palermo, Italy for useful discussions. S.M. and V.M. wish to thank SUMA (INFN – Italy) for partial financial support and the AuroraScience project (funded by PAT and INFN) for allocating the computing resources for this project.

References

[1] M. Jucker and L.C. Walker, Self-propagation of pathogenic protein aggregates in neurodegenerative diseases, Nature, 2013, 501, 45–51.

[2] M. Stefani, Protein misfolding and aggregation: new examples in medicine and biology of the dark side of the protein world, Biochimica et Biophysica Acta, 2004, 1739, 5–25.

[3] D. Selkoe, Folding proteins in fatal ways, Nature, 2003, 426, 900–904.

[4] L. Cruz, B. Urbanc, S. V. Buldyrev, R. Cristie, T. Gomez-Isla, S. Havlin, M. McNamara, H. E. Stanley and B. T. Hyman, Aggregation and disaggregation of senile plaques in Alzheimer disease, Proc. Natl. Acad. Sci. USA, 1997, 94, 7612–7616.

[5] A. J. Baldwin, T. P. J. Knowles, G. G. Tartaglia, A. W. Fitzpatrick, G. L. Devlin, S. L. Shammas, C. A. Waudby, M. F. Mossuto, S. Meehan, S. L. Gras, J. Christodoulou, S. J. Anthony-Cahill, P. D. Barker, M. Vendruscolo and C. M. Dobson, Metastability of native proteins and the phenomenon of amyloid formation, J. Am. Chem. Soc., 2011, 133, 14160–14163.

[6] M. Fandrich, Oligomeric intermediates in amyloid formation: structure determination and mechanisms of toxicity, J. Mol. Biol., 2012, 421, 427–440.

[7] A. L Gharibyan, V. Zamotin, K. Yanamandra, O. S Moskaleva, B. A Margulis, I. A Kostanyan and L. A Morozova-Roche, Lysozyme amyloid oligomers and fibrils induce cellular death via different apoptotic/necrotic pathways, J. Mol. Biol., 2007, 365, 1337–1349.

[8] D. M. Walsh, I. Klyubin, J. V. Fadeeva, W. K. Cullen, R. Anwyl, M. S. Wolfe, M. J. Rowan and D. J. Selkoe, Naturally secreted oligomers of amyloid beta protein potently inhibit hippocampal long-term potentiation in vivo, Nature, 2002, 416, 535–539.

[9] H. A. Pearson and C. Peers, Physiological roles for amyloid β peptides, J. Physiol., 2006, 575.1, 5–10.

[10] A. Schmitz, R. Tikkanen, G. Kirfel and V. Herzog, The biological role of the Alzheimer amyloid precursor protein in epithelial cells, Histochem Cell Biol, 2002, 117, 171–180.

[11] P. Rufenacht, A. Guntert, B. Bohrmann, A. Ducret and H. Dobeli, Quantification of the Aβ peptide in Alzheimer's plaques by laser dissection microscopy combined with mass spectrometry, J. Mass Spectrom., 2005, 40, 193–201.

[12] M. D. Kirkitadze, M. M. Condron and D. B. Teplow, Identification and characterization of key kinetic intermediates in amyloid β-protein fibrillogenesis, J. Mol. Biol., 2001, 312, 1103–1119.

[13] S. Vivekanandan, J. R. Brender, S. Y. Lee and A. Ramamoorthy, A partially folded structure of amyloid-beta(1–40) in an aqueous environment, Biochemical and Biophysical Research Communications, 2011, 411, 312–316.

[14] T. Steckmann, Z. Awan, B. S. Gerstman and P. P. Chapagain, Kinetics of peptide secondary structure conversion during amyloid β-protein fibrillogenesis, Journal of Theoretical Biology, 2012, 301, 95–102.

[15] M. Fandrich, J. Meinhardt and N. Grigorieff, Structural polymorphism of Alzheimer Aβ and other amyloid fibrils, Prion, 2009, 3, 89–93.

[16] A. K. Paravastu, R. D. Leapman, Wai-Ming Yau and R. Tycko, Molecular structural basis for polymorphism in Alzheimer's β-amyloid fibrils, Proc. Natl. Acad. Sci. USA, 2008, 105, 18349–18354.

[17] T. P. J. Knowles, M. Vendruscolo and C. M. Dobson, The amyloid state and its association with protein misfolding diseases, Nature Reviews Molecular Cell Biology, 2014, 15, 384-396.

[18] P. Arosio, M. Vendruscolo, C. M. Dobson, and T. P. J. Knowles, Chemical kinetics for drug discovery to combat protein aggregation diseases, Trends in Pharmacological Sciences, 2014, 35, 127–135.

[19] S. I. A. Cohen, S. Linse, L. M. Luheshi, E. Hellstrand, D. A. White, L. Rajah, D. E. Otzen, M. Vendruscolo, C. M. Dobson and T. P. J. Knowles, Proliferation of amyloid-β42 aggregates occurs through a secondary nucleation mechanism, Proc. Natl. Acad. Sci. USA, 2013, 110, 9758–9763.

[20] P. Arosio, R. Cukalevski, B. Frohm, T. P. J. Knowles and Sara Linse, Quantification of the concentration of Aβ42 propagons during the lag phase by an amyloid chain reaction assay, J. Am. Chem. Soc., 2014, 136, 219–225.

[21] A. Lorenzo and B. A. Yankner, β-Amyloid neurotoxicity requires fibril formation and is inhibited by Congo red, Proc. Natl. Acad. Sci. USA, 1994, 91, 12243–12247.

[22] K. Ono, K. Hasegawa, H. Naiki and M. Yamada, Curcumin has potent anti-amyloidogenic effects for Alzheimer's β-amyloid fibrils in vitro, Journal of Neuroscience Research, 2004, 742–750.

[23] Y. Porat, A. Abramowitz and E. Gazit, Inhibition of amyloid fibril formation by polyphenols: structural similarity and aromatic interactions as a common inhibition mechanism, Chem Biol Drug Des, 2006, 67, 27–37.

[24] A. Sgarbossa, D. Buselli, F. Lenci, In vitro perturbation of aggregation processes in β-amyloid peptides: A spectroscopic study, FEBS Letters, 2008, 582, 3288–3292.

[25] N. Ferreira, S. A. O. Santos, M. R. M. Domingues, M. J. Saraiva and M. R. Almeida, Dietary curcumin counteracts extracellular transthyretin deposition: Insights on the mechanism of amyloid inhibition, Biochimica et Biophysica Acta, 2013, 1832, 39–45.

[26] A. R. A. Ladiwala, J. S. Dordick and P. M. Tessier, Aromatic small molecules remodel toxic soluble oligomers of amyloid through three independent pathways, J. Biol. Chem., 2011, 286, 3209–3218.

[27] X. Meng, L. A. Munishkina, A. L. Fink and V. N. Uversky, Effects of various flavonoids on the α-synuclein fibrillation process, Parkinson's Disease, 2010, doi:10.4061/2010/650794.

[28] F. E. Cohen and J. W. Kelly, Therapeutic approaches to protein misfolding diseases, Nature, 2003, 426, 905-909.

[29] A. Abelein, L. Lang, C. Lendel, A. Gräslund and J. Danielsson, Transient small molecule interactions kinetically modulate amyloid β peptide self-assembly, FEBS Letters, 2012, 586, 3991–3995.

[30] J. M. Mason, N. Kokkoni, K. Stotty and A. J. Doig, Design strategies for anti-amyloid agents, Current Opinion in Structural Biology, 2003, 13, 526–532.

[31] Y. Masuda, M. Fukuchi, T. Yatagawa, M. Tada, K. Takeda, K. Irie, K. Akagi, Y. Monobe, T. Imazawa and K. Takegoshi, Solid-state NMR analysis of interaction sites of curcumin and 42-residue amyloid β-protein fibrils, Bioorg. Med. Chem., 2011, 19, 5967–5974.

[32] L. O. Tjernberg, J. Naslund, F. Lindqvist, J. Johansson, A. R. Karlstrom, J. Thyberg, L. Terenius and C. Nordstedt, Arrest of β-amyloid fibril formation by a pentapeptide ligand, J. Biol. Chem., 1996, 271, 8545–8548.

[33] M. H. Viet, S. T. Ngo, N. S. Lam and M. S. Li, Inhibition of aggregation of amyloid peptides by beta-sheet breaker peptides and their binding affinity, J. Phys. Chem. B, 2011, 115, 7433–7446.

[34] P. Giannozzi, K. Jansen, G. La Penna, V. Minicozzi, S. Morante, G. C. Rossi and F. Stellato, Zn induced structural aggregation patterns of β-amyloid peptides by first-principle simulations and XAS measurements, Metallomics, 2012, 4, 156–165.

[35] Y. Miller, B. Ma and R. Nussinov, Zinc ions promote Alzheimer Aβ aggregation via population shift of polymorphic states, Proc. Natl. Acad. Sci. USA, 2010, 107, 9490-9495

[36] P. A. Novick, D. H. Lopes, K. M. Branson, A. Esteras-Chopo, I. A. Graef, G. Bitan and V. S. Pande, Design of β-amyloid aggregation inhibitors from a predicted structural, Motif. J. Med. Chem., 2012, 55, 3002–3010

[37] V. Minicozzi, R. Chiaraluce, V. Consalvi, C. Giordano, C. Narcisi, P. Punzi, G.C. Rossi and S. Morante, Computational and experimental studies on β-sheet breakers targeting $A\beta_{1-40}$ fibrils, J. Biol. Chem., 2014, 289, 11242-11252.

[38] M. D'Amico, M. G. Di Carlo, M. Groenning, V. Militello, V. Vetri and Maurizio Leone, Thioflavin T promotes Aβ(1−40) amyloid fibrils formation, J. Phys. Chem. Lett., 2012, 3, 1596−1601.

[39] S. Vilasi, R. Sarcina, R. Maritato, A. De Simone, G. Irace, I. Sirangelo, Heparin Induces Harmless Fibril Formation in Amyloidogenic W7FW14F Apomyoglobin and Amyloid Aggregation in Wild-Type Protein In Vitro, PLoS ONE, 2011, 6, e22076.

[40] Grelle, G.; Otto, A.; Lorenz, M.; Frank, R. F.; Wanker, E. E.; Bieschke, J. Black Tea Theaflavins Inhibit Formation of Toxic Amyloid-β and α-Synuclein Fibrils, Biochemistry, 2011, 50, 10624−10636.

[41] H. A. Lashuel, D. M. Hartley, D. Balakhaneh, A. Aggarwal, S. Teichberg, D. J. E. Callaway, New Class of Inhibitors of Amyloid-β Fibril Formation, J. Biol. Chem., 2002, 277, 42881−42890.

[42] Y. Fezoui, D. Hartley, J. Harper, D. Khurana, R. Walsh, M. M. Condron, D. Selkoe, P. T. J. Lansbury, A. Fink and D. B. Teplow, An improved method of preparing the amyloid β-protein for fibrillogenesis and neurotoxicity experiments, Amyloid, 2000, 7, 166−178.

[43] V. Foderà, S. Pagliara, O. Otto, U. F. Keyser and A. M. Donald, Microfluidics reveals a flow-induced large-scale polymorphism of protein aggregates, J. Phys. Chem. Lett. 2012, 3, 2803−2807.

[44] B. Hess, C. Kutzner, D. van der Spoel and E. Lindahl, GROMACS 4: Algorithms for highly efficient, load-balanced, and scalable molecular simulation, J. Chem. Theory Comput., 2008, 4, 435–447.

[45] C. Oostenbrink, A. Villa, A. E. Mark and W. F. Van Gunsteren, A biomolecular force field based on the free enthalpy of hydration and solvation: The GROMOS force-field parameter sets 53A5 and 53A6, J. Comput. Chem., 2004, 25, 1656–1676.

[46] Stacey R. Gerben, Justin A. Lemkul, Anne M. Brown and David R. Bevan, Comparing atomistic molecular mechanics force fields for a difficult target: a case study on the Alzheimer's amyloid β-peptide. Journal of Biomololecular Structure and Dynamics, 2014, 32, 1817-1832.

[47] G. Bussi, D. Donadio and M. Parrinello, Canonical sampling through velocity rescaling, J. Chem. Phys., 2007, 126, 014101.

[48] H.J.C. Berendsen, J.P.M. Postma, A. DiNola and J.R. Haak, Molecular dynamics with coupling to an external bath, J. Chem. Phys., 1984, 81, 3684–3690.

[49] A.K. Malde, L. Zuo, M. Breeze, M. Stroet, D. Poger, P.C. Nair, C. Oostenbrink and A.E. Mark, An Automated force field Topology Builder (ATB) and repository: version 1.0, J Chem. Theo. Comp., 2011, 7, 4026–4037.

[50] T. Darden, D. York and L. Pedersen, Particle mesh Ewald: An Nlog(N) method for Ewald sums in large systems, J. Chem. Phys., 1993, 98, 10089–10092.

[51] G. Sancataldo, V. Vetri, V. Foderà, G. Di Cara, V. Militello, and M. Leone, Oxidation Enhances Human Serum Albumin Thermal Stability and Changes the Routes of Amyloid Fibril Formation, PLoS ONE, 2014, 9: e84552. doi:10.1371/journal.pone.0084552

[52] J.R. Lakowicz, Principles of Fluorescence Spectroscopy 3rd ed., Springer, 2006

[53] V R. Carrotta, V. Vetri, F. Librizzi, V. Martorana, V. Militello and M. Leone, Amyloid Fibrils Formation of Concanavalin A at Basic pH J. Phys. Chem B, 2011, 115 (12), 2691-2698.

[54] R. F. Pasternack, C. Fleming, S. Herring, P. J. Collings, J. dePaula, G. DeCastro and E. J. Gibbs, Aggregation kinetics of extended porphyrin and cyanine dye assemblies, Biophysical Journal, 2000, 79, 550–560.

[55] K. Ono, M. M. Condron and D. B. Teplow, Structure–neurotoxicity relationships of amyloid β-protein oligomers, Proc Natl Acad Sci U S A, 2009, 106, 14745-14750.

[56] K. Ono, M. M. Condron and D. B. Teplow, Effects of the English (H6R) and Tottori (D7N) familial Alzheimer disease mutations on amyloid β-protein assembly and toxicity, J. Biol. Chem., 2010, 285, 23186-23197.

[57] S. I. A. Cohen, M. Vendruscolo, C. M. Dobson and T. P. J. Knowles, From macroscopic measurements to microscopic mechanisms of protein aggregation, J. Mol. Biol., 2012, 421, 160–171.

[58] P. Arosio, R. Cukalevski, B.Frohm, T. P. J. Knowles, and S. Linse, Quantification of the Concentration of Aβ42 Propagons during the Lag Phase by an Amyloid Chain Reaction Assay J. Am. Chem. Soc., 2014 136 (1), 219-225

[59] H. G. Kapitza, G. McGregor and K. A. Jacobson, Direct measurement of lateral transport in membranes by using time-resolved spatial photometry, Proc. Natl. Acad. Sci. USA, 1985, 82, 4122-4126.

[60] P. Hortschansky, V. Schroeckh, T. Christopeit, G. Zandomeneghi and M. Fandrich, The aggregation kinetics of Alzheimer's β-amyloid peptide is controlled by stochastic nucleation, Protein Science, 2005, 14, 1753-1759.

[61] V. Foderà, S. Cataldo, F. Librizzi, B. Pignataro, P. Spiccia and M. Leone, Self-organization pathways and spatial heterogeneity in insulin amyloid fibrils formation, J. Phys. Chem. B, 2009, 113, 10830–10837.

[62] F. A. Ferrone, J. Hofrichter and W. A. Eaton, Kinetics of sickle hemoglobin polymerization. II. A double nucleation mechanism, J. Mol. Biol., 1985, 183, 611–631.

[63] F. A. Ferrone, J. Hofrichter, H. R. Sunshine and W. A. Eaton, Kinetic studies on photolysis-induced gelation of sickle cell hemoglobin suggest a new mechanism, Biophys. J., 1980, 32, 361-380.

[64] M. B. Borgia, A. A. Nickson, J. Clarke and M. J. Hounslow, Mechanistic model for amorphous protein aggregation of immunoglobulin-like domains, J. Am. Chem. Soc., 2013, 135, 6456−6464.

[65] O. Crescenzi, S. Tomaselli, R. Guerrini, S. Salvadori, P.A. Temussi and D. Picone, Solution structure of the Alzheimer's disease Amyloid beta peptide(1-42), Eur. J. Biochem., 2002, 269, 5642–5648.

[66] V.N. Maiorov and G.M. Crippen, Size-independent comparison of protein three-dimensional structures. Proteins, 1995, 22, 273–283.

[67] J. Khandogin and C.L. Brooks III, Linking folding with aggregation in Alzheimer's β-amyloid peptides, PNAS, 2007, 104, 16880-16885.

[68] R. Azriel and E. Gazit, Analysis of the structural and functional elements of the minimal active fragment of islet amyloid polypeptide (IAPP) - An experimental support for the key role of the phenylalanine residue in amyloid formation. J Biol Chem, 2001, 276, 34156–34161

[69] W. Kabsch and C. Sander, Dictionary of protein secondary structure: Pattern recognition of hydrogen-bonded and geometrical features. Biopolymers, 1983, 22, 2577–2637.

[70] M. Biancalana and S. Koide, Molecular mechanism of Thioflavin-T binding to amyloid fibrils, Biochimica et Biophysica Acta (BBA) - Proteins and Proteomics 2010, 1804, 1405–1412

[71] A. Päiviö,E. Nordling, Y. Kallberg, J. Thyberg and J. Johansson, Stabilization of discordant helices in amyloid fibril-forming proteins, Protein Sci., 2004,13, 1251-1259.

Figure 1. A: Normalized Rayleigh scattering intensity at 435 nm as a function of time for Aβ(1-40) samples at three different temperatures. The peptide was dissolved in 50 mM sodium phosphate buffer, pH 7.4, containing 33 μM of ThT, to a final concentration of 120 μM; **B**: ThT fluorescence intensity as a function of time acquired simultaneously to Rayleigh scattering. The fluorescence curves were normalized to the ThT fluorescence intensity value after 3 hours of incubation in order to compare the temporal profiles. Pink solid line indicates the stretched exponential fit (see text). Vertical dashed lines correspond to the end of the lag-phase (t_0) for the three temperatures.

Figure 2. A, **B**, **C** and **D**: Representative transmission electron microscopy measurements on Aβ(1-40) samples prepared dissolving the peptide in 50 mM sodium phosphate buffer, pH 7.4, with (**A** and **B**) and without (**C** and **D**) the addition of 30 μM of ThT. The inset scale bar in panel **D** is 2 μm. **E**: Far-UV CD spectra acquired at RT for Aβ(1-40) sample before and after 45 hours of thermal incubation at 41°C. The spectrum of an identical sample without ThT addition is also reported for comparison. Panel **F**: 512X512 confocal image of the edge of a drop of an Aβ(1-40) sample identical to that one in panels C and D. This sample was incubated at 41 °C and images acquired during the first stage of the kinetics. Panel **G**: Typical Fluorescence recovery profile obtained from FRAP experiments on a circular region of 20 μm radius (ROI-1) on sample in panel E.

Figure 3. A: Rayleigh scattering intensity at 435 nm as a function of time for Aβ (1-40) samples at different peptide concentrations, incubated at 41 °C. The peptide was dissolved in 50 mM sodium phosphate buffer, pH 7.4, containing 28 μM of ThT. Inset: Rayleigh scattering intensity at 435 nm as a function of time for Aβ (1-40) samples containing 33 μM of ThT, incubated at 37 °C. **B**: ThT fluorescence intensity as a function of time simultaneously acquired to Rayleigh scattering in panel A. Inset: ThT fluorescence intensity as a function of time simultaneously acquired to Rayleigh scattering in the inset of panel A.

Figure 4. A) Aβ(1-40) peptide RMSD(t) in the absence (green) and in the presence (magenta) of ThT molecules along the 90 ns NpT simulation. The dark cyan area indicates the initial equilibration time. B) Mobility of Aβ(1-40) residues. Color code is as before. Only the last 60 ns of the simulation was used.

Figure 5. ThT molecules whose center of mass is within 8 Å from the Aβ(1-40) backbone atoms as a function of simulation time. For readers convenience we write here the Aβ(1-40) amino acid sequence DAEFRHDSGYEVHHQKLVFFAEDVGSNKGAIIGLMVGGVV

Figure 6. Aβ(1-40) DSSP secondary structure as function of simulation time in the absence (panel A) and in the presence (panel B) of ThT. The tridimensional structure of the most representative configuration of each 10 ns simulation are drawn as cartoons.

Figure 7. 3D drawing of the Aβ(1-40)-ThT representative structure of the last 10 ns of Molecular Dynamic Simulation. This could indicate an higher affinity of the ThT induced conformation with further ThT molecules.

Table 1. Relative secondary structure content computed for Aβ(1-40) and Aβ(1-40)-ThT systems along the final simulated 60 ns. In red are indicated significant changes induced by ThT.